26th INTERNATIONAL CONGRESS ON SOUND AND VIBRATION
7-11 July 2019, Montreal

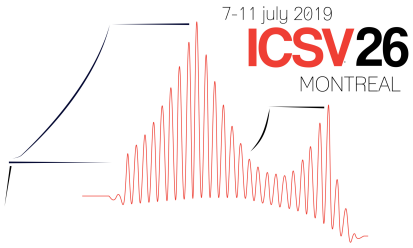

ACTIVE SIDEWALL PANELS WITH REMOTE MICROPHONE TECHNIQUE FOR AIRCRAFT INTERIOR NOISE REDUCTION

Malte Misol
German Aerospace Center, Institute of Composite Structures and Adaptive Systems, Braunschweig, Germany
email: malte.misol@dlr.de

The main issue of this contribution is the reduction of aircraft interior noise by means of actively controlled sidewall panels (linings). It was shown in prior work that considerable reductions of interior sound pressure level can be achieved using structural actuators on the lining and microphones distributed in the seat area in front of the linings. The use of microphones is undesirable for several reasons and it contradicts the aim of a fully integrated and autonomous lining module (smart lining). Therefore, the present contribution aims at the replacement of the error microphones by a number of structural sensors and an acoustic filter. This method is called the remote microphone technique for active control. Several steps are undertaken to define the smart lining with remote microphones. The whole work is based on experimental data of a double panel system mounted in a sound transmission loss facility. A multi-tonal acoustic excitation, typical for a counter rotation open rotor (CROR) engine, is used as the load case for the definition of the actuators and a broadband acoustic excitation, is used as the load case for the definition of structural sensors. 19 Accelerometers are mounted on the lining and 20 microphones are placed in front of it. All sensor signals are sampled simultaneously for deterministic and broadband load cases. The lining is equipped with two inertial mass actuators at fixed positions which are used for the active control. The measurement data is used for the derivation of an observer and for the simulation of a smart lining with remote microphones.

Keywords: aircraft, interior noise, active control, remote microphone technique, lining

1. Introduction

The active control of rotor noise in aircraft has been pursued for more then thirty years and several systems have been successfully implemented (e.g. the aircraft Saab 2000 or Bombardier Dash 8 Q 400). A common solution uses loudspeakers in the cabin to reduce the interior sound pressure by so-called anti-sound (ANC). Early results of ANC in aircraft are documented by Elliott et al. [1]. There, maximum sound pressure level (SPL) reductions of 13 dB at the fundamental blade passage frequency (88 Hz) are reported. An alternative approach is the active structural acoustic control (ASAC) of the fuselage by means of shakers or piezoelectric patch actuators. Early results on ASAC in aircraft are documented by Fuller and Jones [2]. A similar approach for active interior noise reduction uses active trim panels (linings) instead of actuated fuselage structures. In the experimental work of Lyle and Silcox [3], the active linings are coupled to a stiffened fuselage barrel. The excitation of the fuselage barrel is realized with a loudspeaker. The active linings achieve a global SPL reduction of up to 5 dB. In Tran and Mathur [4],

full-scale experiments in a McDonnell Douglas DC-9 aircraft (on ground) are described. The active control system uses 16 piezoelectric patch actuators on the linings (aft section) and 32 microphones placed at the headrests and in the aisle. The measured noise reduction is basically limited to one frequency (out of eight), which is unsatisfactory compared to loudspeaker-based systems (ANC) and systems with actuators on the fuselage that were implemented on the same aircraft (see [4, Fig. 4]). Recent results on aircraft interior noise reduction with active linings are published by Misol et al. [5, 6]. Firstly, a serial production Airbus A350 lining augmented with actuators, sensors and an active control system is tested in a sound transmission loss facility [5]. Secondly, full-scale tests of two active lining modules mounted in the cabin of a Dornier Do728 aircraft are reported in Misol [6]. In both cases the acoustic effect of the rotor engines on the fuselage is mimicked by means of a loudspeaker array. A maximum (mean) SPL reduction of 11.3 dB (6.8 dB) is achieved in the Do728 cabin in front of the active linings. All of the mentioned active noise control systems have in common that they use microphones as error sensors. These microphones are distributed all over the cabin which is considered undesirable because it contradicts the approach of the so-called smart lining concept followed by Misol et al. [7]. Therefore, the remote microphone technique (RMT) for active control [8] is applied to substitute the error microphones. The RMT uses accelerometers on the lining in combination with an observer filter within the controller [9]. Whereas in Roure and Albarazzin [8] remote microphones are used for the estimation of the error signals, Cheer and Daley [9] use accelerometers mounted on the radiating structure for this task. The latter approach is also followed here, because it allows to structurally integrate the sensors into the lining, which is fully in line with the smart lining concept. The present contribution focuses on the noise reduction capability of an active lining system using the RMT. Simulations are performed based on measurement data of the Airbus A350 lining system formerly described in [5].

2. Experimental setup

Figure 1 shows a scheme of the experimental setup in a sound transmission loss facility. The loudspeaker array (LSA) is placed in front of the fuselage structure with approx. 0.15 m offset. In total 72 loudspeakers arranged in an array of nine rows and eight columns are used for the disturbance excitation. Two different acoustic load cases are considered. Firstly, the lowest five harmonics of a counter rotation open rotor (CROR) engine (119.4 Hz, 149.2 HZ, 268.6 Hz, 388 Hz and 417.9 Hz) are synthesized (see Algermissen et al. [10] for further information) and secondly, all 72 loudspeakers are controlled with uncorrelated bandlimited white noise signals resulting in a spatially weakly correlated broadband excitation. The test specimen consisting of a carbon fiber reinforced plastics (CFRP) fuselage structure and a coupled lining is mounted in the test opening of the facility. Figure 2 shows the experimental setup seen from the semi-anechoic room. The fuselage structure is elastically supported by means of shock mounts placed at the outer frames one in each corner (see yellow boxes in Fig. 2 (b)). From a total of 19 accelerometers (blue boxes), 16 are selected as potential remote sensors for the RMT (the discarded ones are marked with an X). The actuator locations are kept constant at the indicated positions (red boxes). The 20 microphones (green boxes) are arranged in two lines as shown in Fig. 2 (b). It is assumed that the vertical ear locations of passengers sitting in an aircraft will usually be between these two lines. The microphones are placed in three distances from the lining to capture SPL variations from the window seats to the aisle seats. The signals of all sensors indicated in Fig. 2 plus a reference signal from the LSA and the two actuator control voltages are sampled simultaneously for 100 s with a sampling rate of 5kHz. Time data of the structural and the acoustic disturbances from all sensors is sampled with the LSA switched on (either CROR or white noise). Time data of the CROR load case is used for the identification of the observer filter and for the simulation of the active control system with RMT. Time data of the white noise load case is used for the selection of the remote sensors. Time data for the calculation of the

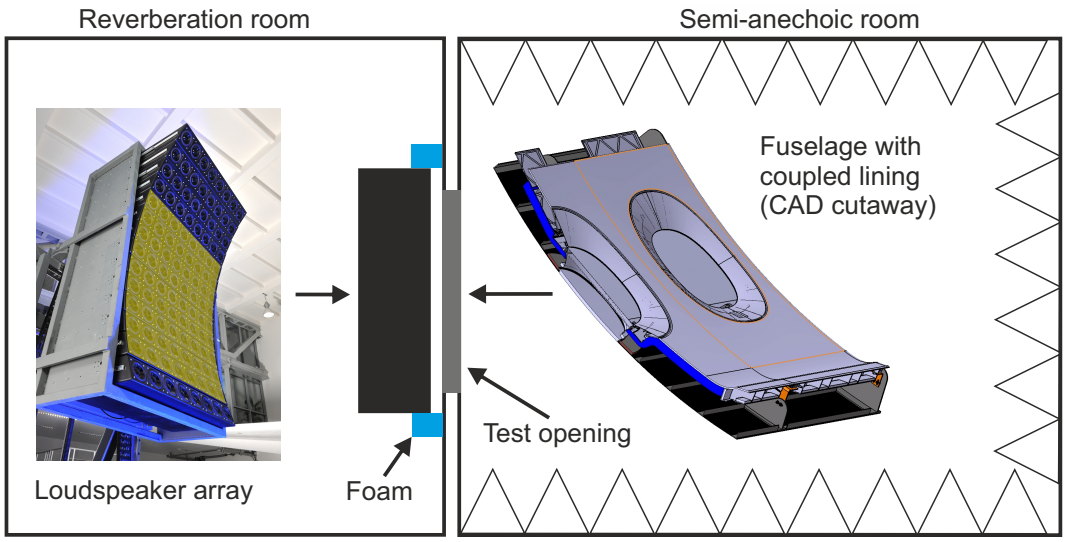

Figure 1: Top view schematic of the experimental setup in the transmission loss facility showing the loudspeaker array in the reverberation room and the fuselage lining-system mounted in the test opening between reverberation and semi anechoic room. The selected loudspeaker area is highlighted in yellow. The gap between the fuselage structure and the loudspeaker array is proofed with foam to reduce reverberation.

actuator frequency response functions (FRF) is obtained when the LSA is switched off and the actuators are supplied with uncorrelated bandlimited white noise signals. More information on how the time data is used will be provided in subsequent sections.

3. Sensors and actuators

Two different load cases are assumed for the definition of the remote sensors and the actuators. Regarding the sensors, the broadband excitation is the defining load case whereas the actuators are dimensioned for the CROR load case. In both cases the number of transducers is the main parameter, although the position has an impact too. Theoretically, for the deterministic CROR load case, a single remote sensor is sufficient to estimate the pressure at the virtual locations. However, the use of a single remote sensor is considered unreasonable with regard to robustness because its failure would tie the whole system. Furthermore, in the broadband case with multiple independent noise sources, an accurate pressure estimate requires a sufficient number of remote sensors. A quantification of sufficiency is provided by the multiple coherence function. Therefore, it is applied as a metric to, firstly, define the required number and, secondly, the best combination of remote sensors. In Eq. (1), $\mathbf{x}$ is the vector of accelerometer signals and y is the sound pressure at one of the 60 microphone positions. The spectra of these signals are denoted by $\mathbf{X}$ and Y.

$$\bar{C} = \frac{1}{n_2 - n_1 + 1} \sum_{k=n_1}^{n_2} \frac{\mathbf{S}_{xy}(k)\mathbf{S}_{xx}^{-1}(k)\mathbf{S}_{xy}^{H}(k)}{S_{yy}(k)} \tag{1}$$

The multiple coherence function, which is a frequency dependent real number between zero and one, will be averaged twice. First, over the discrete frequency k leading to $\bar{C}$ as given by Eq. (1) and second, over all 60 microphone positions leading to $\bar{C}_{avg}$. With the chosen frequency resolution of 4 Hz

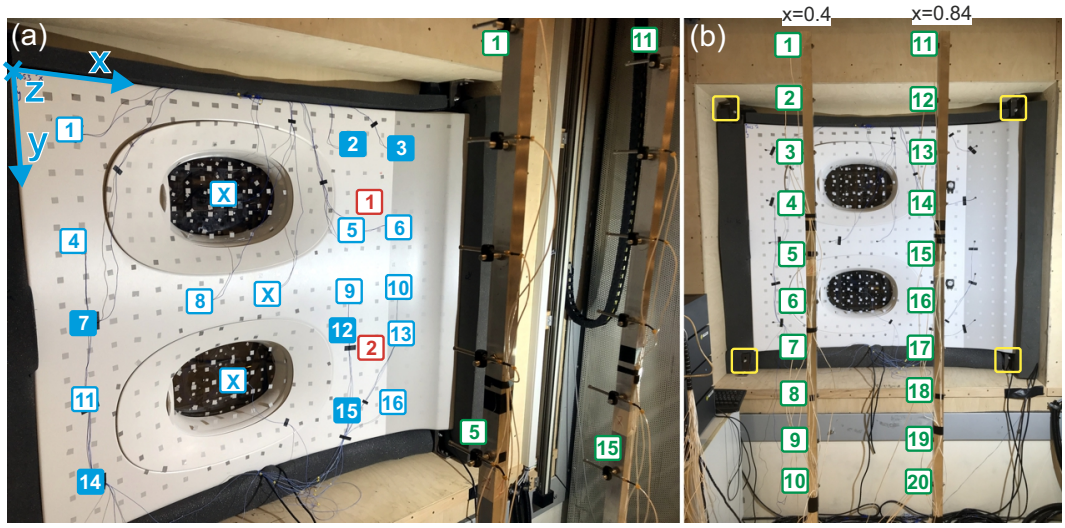

Figure 2: Experimental setup in the transmission loss facility seen from the semi anechoic room. The accelerometers are indicated with blue, the actuators with red and the microphones with green boxes. The accelerometers chosen for the observer of the remote microphone method are 2, 3, 7, 12, 14, 15. The microphones are positioned $z = -0.5\,m$, $z = -1\,m$ or $z = -1.5\,m$ in front of the lining along two vertical lines at $x = 0.4\,m$ and $x = 0.84\,m$ spanning two surfaces used for control performance evaluation.

the summation indices in Eq. (1) are $n_1 = 13$ and $n_2 = 125$. The power spectral densities (PSD) $\mathbf{S}_{xy} = E\{Y\mathbf{X}^H\}$, $\mathbf{S}_{xx} = E\{\mathbf{X}\mathbf{X}^H\}$ and $S_{yy} = E\{YY^H\}$ are calculated with 79 spectral averages for the broadband load case. A target value of $\bar{C}_{avg} = 0.8$ is predefined which corresponds to an explanation of roughly 90% of the SPL by the remote sensors. An initial calculation of $\bar{C}$ for different sensor configurations suggests a number of six accelerometers. The best combination of six sensors out of 16 is found by combinatorics. The complete optimization run requires 8008 calculations of $\bar{C}_{avg}$. The selected combination of six accelerometers (see Fig. 2 (a)) has an average mean coherence of $\bar{C}_{avg} = 0.8021$ compared to the worst combination having only $\bar{C}_{avg} = 0.7488$. The observer filter $\mathbf{O}$ is defined by the FRF matrix of the vector of accelerometer signals $\mathbf{x}$ and the vector of microphone signals $\mathbf{y}$ measured with CROR excitation. The PSD are defined as above but with $\mathbf{Y}$ being a vector.

$$\mathbf{O}(k) = \mathbf{S}_{xy}(k)\mathbf{S}_{xx}^{-1}(k) \tag{2}$$

Here, only the five frequency lines corresponding to the CROR frequencies are relevant. Alternative forms of $\mathbf{O}$ having a diagonal structure or being a fully populated matrix are mentioned in Roure and Albarazzin [8].

The actuator locations are not optimized, but the required number is estimated by the identified actuator FRF $\hat{\mathbf{G}}_a$ and the disturbance sound pressure levels $\mathbf{D}_a$ measured with CROR excitation from the LSA. The SPL produced by the LSA in front of the fuselage is roughly 113 dB. Although the SPL of a real CROR engine is unknown, it is assumed to be significantly higher (130 dB or more). In the experiments two actuators of the type Visaton EX 45 S (10 W, 8 Ω, $V_{max} = 8.9\,V$, 60 g) are attached to the lining (see Fig. 2). The calculation of the control voltage $\mathbf{U}$ needed to counteract the CROR induced pressure field

in front of the lining results from Eq. (3).

$$\mathbf{D}_a(k) \stackrel{!}{=} \hat{\mathbf{Y}}_\mathbf{a} = \hat{\mathbf{G}}_a(k)\mathbf{U}(k) \rightarrow \mathbf{U}(k) = \left[\hat{\mathbf{G}}_a(k)^H \hat{\mathbf{G}}_a(k)\right]^{-1} \hat{\mathbf{G}}_a(k)^H \mathbf{D}_a(k) \tag{3}$$

The inverse Fourier transform of $\mathbf{U}$ containing the values from Eq. (3) for the five CROR frequency lines yiels the control voltage $\mathbf{u}(t)$ in the time domain. It turns out that the required maximum voltage is 0.924 V which is far below the maximum value of 8.9 V. With a safety factor of two, the actuator stroke margin is 13.7 dB and maximum exterior SPL of roughly 125 dB can be handled by the two actuators. If higher SPL are to be counteracted, more and/or heavier actuators can be used. An optimization study (not described here) suggests that the chosen actuator locations are highly suitable and, furthermore, that not much benefit is gained from a position optimization compared to an educated guess.

4. Simulation

The simulation scheme of the adaptive controller with RMT is shown in Fig. 3. It consists of the observer $\mathbf{O}$ from Eq. (2) in the upper and the adaptive controller $\mathbf{W}$ with least mean squares (LMS) algorithm in the lower part. Time domain quantities are in lowercase and frequency domain quantities are in uppercase. Estimated quantities are indicated by a hat above the symbol to discriminate them from the real (ideal) values. The input data for the simulation $\mathbf{d}_s$, $\mathbf{x}$ and $\mathbf{d}_a$ (green blocks) is obtained from measurement of the CROR load case. The vector $\mathbf{d}_s$ contains the sampled time sequences of the selected remote sensors (accelerometers). The scalar reference signal from the LSA containing the five CROR harmonics is denoted by x. The vector $\mathbf{d}_a$ contains the sampled time sequences of all 60 microphones. The real error signal $\mathbf{e}_a$ results from subtracting the secondary pressure signals $\hat{\mathbf{y}}_a$ from the disturbance pressure signals $\mathbf{d}_a$. It is assumed that the estimated actuator FRF matrix $\hat{\mathbf{G}}_a$ perfectly matches the unknown real actuator FRF matrix $\mathbf{G}_a$ and hence $\hat{\mathbf{y}}_a$ equals $\mathbf{y}_a$. Furthermore, it is assumed that the actuator feedback on the remote sensors is ideally cancelled by a perfect plant model and therefore, this effect is not reflected in the simulation scheme. Insofar, the simulation results are to be considered as the upper limit of SPL reduction for the system under consideration. For the multi-tonal CROR load case it is reasonable to implement the adaptive controller with RMT in the frequency domain. The control algorithm is adopted from Johansson et al. [11]. It is based on a complex filtered-x LMS algorithm, which realizes a narrowband multiple-reference feedforward controller. The blocks $t \rightarrow F$ transform a real input of dimension N into a complex output of dimension $N \times R$. Here, with $R = 5$ harmonics, the dimension of the output is multiplied by five. Hence, the scalar reference signal x is mapped to the vector $\mathbf{X}$ containing the five scalar complex reference signals X_r. Accordingly, the actuator FRF matrix $\hat{\mathbf{G}}_a$ is split into five complex matrices $\hat{\mathbf{G}}_a^r$. With this algorithm each actuator is individually controlled by one adaptive complex finite impulse response (FIR) filter weight per frequency. The time dependence is denoted by index n. Here, $\mathbf{W}_r$ contains the two filter weights for harmonic r. The square $J(n) = |\hat{\mathbf{e}}_a(n)|^2$ of the estimated error signal vector (cp. Fig. 3)

$$\begin{aligned} \hat{\mathbf{e}}_a(n) &= \hat{\mathbf{d}}_a(n) - \sum_{r=1}^{R} \Re\left\{\hat{\mathbf{G}}_a^r \mathbf{U}_r(n)\right\} \\ &= \hat{\mathbf{d}}_a(n) - \sum_{r=1}^{R} \Re\left\{\hat{\mathbf{G}}_a^r \mathbf{W}_r(n) X_r(n)\right\}, \quad \text{with} \quad \mathbf{U}_r = \mathbf{W}_r X_r, \end{aligned} \tag{4}$$

should be minimized by the filtered-x LMS algorithm. The adaptation of the weight vectors

$$\mathbf{W}_r(n+1) = \mathbf{W}_r(n) - \mathbf{M}_r \frac{\partial J(n)}{\partial \overline{\mathbf{W}}_r} = \mathbf{W}_r(n) + \mathbf{M}_r 2\overline{X}_r(n)\{\hat{\mathbf{G}}_a^r\}^H \hat{\mathbf{E}}_a^r(n) \tag{5}$$

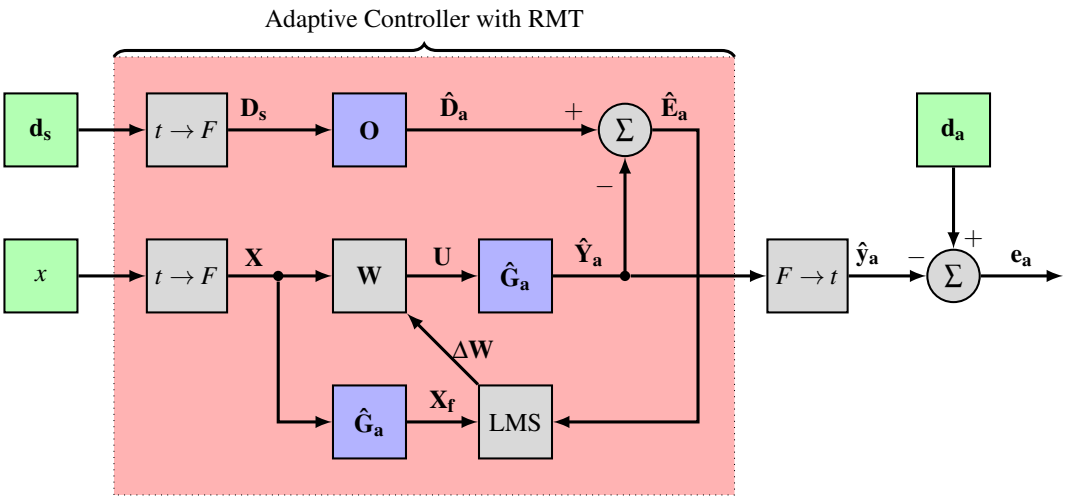

Figure 3: Block diagram of the simulation scheme of adaptive controller with RMT.

is done using $\mathbf{M}_r = \mu_0 \left(\rho_r \text{diag} \left(\{\hat{\mathbf{G}}_a^r\}^H \hat{\mathbf{G}}_a^r \right) \right)^{-1}$ with $\rho_r = E\{|X_r(n)|^2\}$ and $\mu_0 < 1$. The results presented in the next section are based on the evaluation of $\mathbf{d}_a$ and $\mathbf{e}_a$.

5. Results

Results are provided for two different virtual microphone configurations (see caption of Fig. 4). In both cases the control performance is evaluated by taking the average SPL of all 60 microphones. Configuration one achieves a mean SPL reduction of 6.4 dB (3.8 dB(A)) and a maximum SPL reduction of 17 dB or (13 dB(A)). Configuration two achieves a mean SPL reduction of 7.9 dB (5.2 dB(A)) and a maximum SPL reduction of 12 dB (11 dB(A)). Since configuration two uses virtual microphones in both planes, it achieves a more homogenous SPL reduction then configuration one. This is reflected in an increased mean and a decreased maximum SPL reduction. Figure 4 shows the SPL distribution in front of the lining evaluated on two planes (see caption of Fig. 4). The plots in the first row of Fig. 4 visualize the decrease of the disturbance SPL in the negative z-direction with maximum SPL at the two window positions near the lining at $z = -0.5\ m$ and minimum SPL remote of the lining at $z = -1.5\ m$. The second and the third row of Fig. 4 document a significant and uniform SPL reduction achieved by the active control system. Whereas the results in the plane at $x = 0.4\ m$ are similar in both configurations, the average SPL reduction in the plane at $x = 0.84\ m$ is increased for the second configuration. Both configurations require the same number of physical sensors (six) and the same number of complex filter weights (ten). Only the row dimension of the observer $\mathbf{O}$ and the actuator FRF matrix $\hat{\mathbf{G}}_a$ increase with the number of virtual sensors.

6. Conclusion and outlook

In this work the remote microphone technique for active control is applied to a double panel aircraft fuselage structure mounted in a sound transmission loss facility. Simulations are performed based on measurement data and identified plant models. The considered CROR load case contains the first five most harmful rotor harmonics (119.4 Hz, 149.2 HZ, 268.6 Hz, 388 Hz and 417.9 Hz). Global SPL reductions up to 7.9 dB are achieved for a regular distribution of 30 virtual microphones in an area of

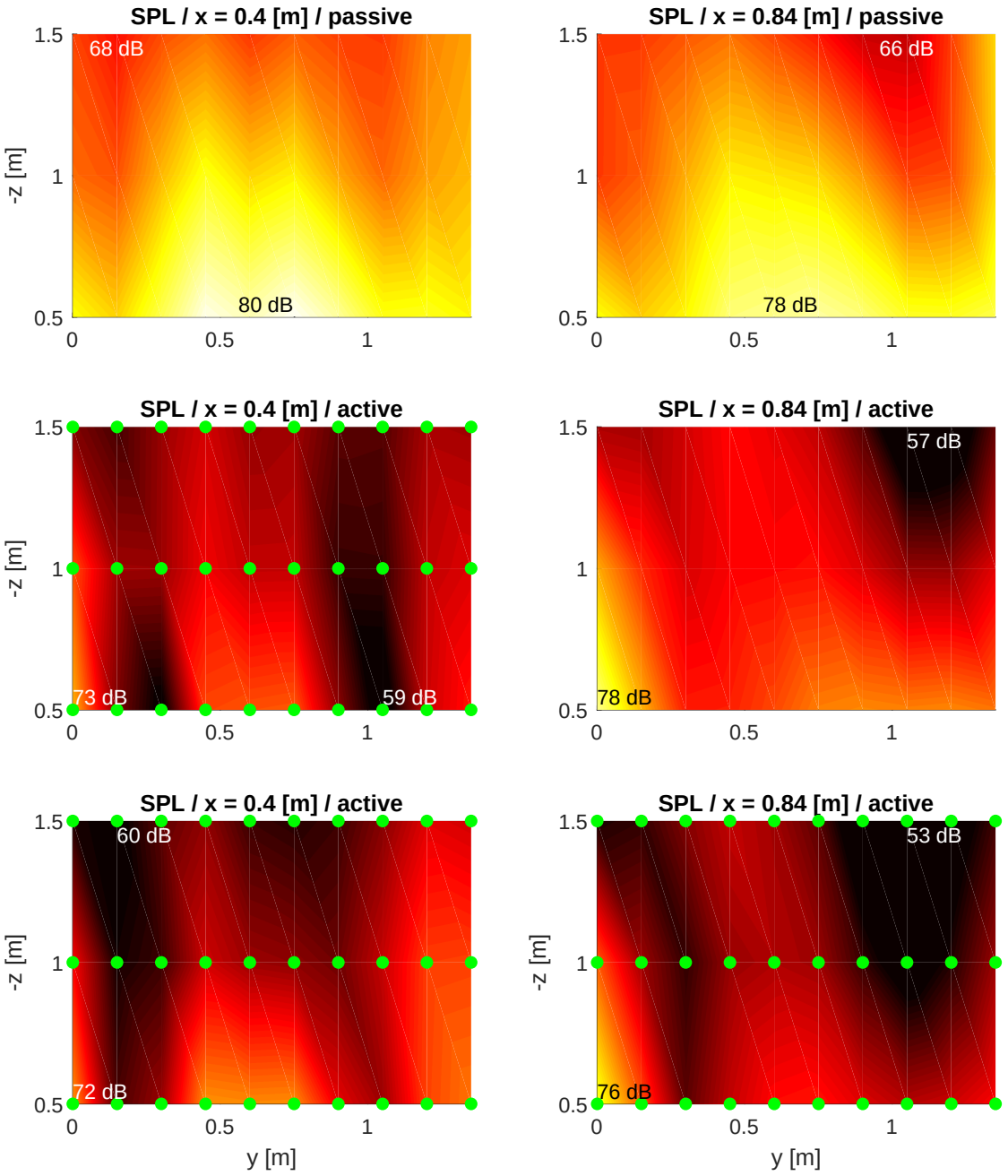

Figure 4: Sound pressure level distribution in front of the lining evaluated on two planes (see Fig. 2(b)). Results without active control (passive) are shown in the first row. Results of the active control with 30 remote microphones (green dots) located in one plane (configuration one) are shown in the second row. Results of the active control with 60 remote microphones distributed over two planes (configuration two) are shown in the third row. The maximum and minimum SPL are indicated in each plot.

$1.35 \times 1.5\ m^2$ and for a regular distribution of 60 virtual microphones in a volume of $1.35 \times 1.5 \times 0.44\ m^3$. Current and future work focuses on the integration of actuators, sensors and wiring into the lining structure and on the robustness and the numerical efficiency of the control algorithm.

7. Acknowledgements

The research work documented in this manuscript is part of the project Advanced Concepts for Aero-Structures with Integrated Antennas and Sensors (ACASIAS) funded by the European Union under grant agreement number 723167. The author gratefully acknowledges the support of Dietmar Völkle, Markus Klingseis, Florian Hesselbach and Alexander Rehmann from DIEHL Aviation Laupheim.

References

1. Elliott, S. J., Nelson, P. A., Stothers, I. M. and Boucher, C. C. In-flight experiments on the active control of propeller-induced cabin noise, *Journal of Sound and Vibration*, **140** (2), 219–238, (1990).

2. Fuller, C. R. and Jones, J. D. Experiments on reduction of propeller induced interior noise by active control of cylinder vibration, *Journal of Sound and Vibration*, **112** (2), 389–395, (1987).

3. Lyle, K. H. and Silcox, R. J. A study of active trim panels for interior noise reduction in an aircraft fuselage, *SAE Technical Paper*, 05, SAE International, (1995).

4. Tran, B. N. and Mathur, G. P. Aircraft interior noise reduction tests using active trim panels, *Proceedings of Noise-Con 96*, pp. 395–400, (1996).

5. Misol, M., Haase, T., Algermissen, S., Papantoni, V. and Monner, H. P. Lärmreduktion in Flugzeugen mit aktiven Linings, *Smarte Strukturen und Systeme – Tagungsband des 4SMARTS-Symposiums*, pp. 329–339, (2017).

6. Misol, M. Experiments on noise reduction in aircraft with active sidewall panels, *25th International Congress on Sound and Vibration*, pp. 1–7, Silesian University of Technology Press, (2018).

7. Misol, M., Algermissen, S., Rose, M. and Monner, H. P. Aircraft lining panels with low-cost hardware for active noise reduction, *Joint Conference ACOUSTICS 2018*, (2018).

8. Roure, A. and Albarrazin, A. The remote microphone technique for active noise control, Douglas, S. (Ed.), *PROCEEDINGS OF ACTIVE 99: THE INTERNATIONAL SYMPOSIUM ON ACTIVE CONTROL OF SOUND AND VIBRATION, VOLS 1 & 2*, pp. 1233–1244, (1999).

9. Cheer, J. and Daley, S. Active structural acoustic control using the remote sensor method, *Journal of Physics: Conference Series*, **744** (1), (2016).

10. Algermissen, S., Meyer, S., Appel, C. and Monner, H. P. Experimental synthesis of sound pressure fields for active structural acoustic control testing, *Journal of Intelligent Material Systems and Structures*, (2013).

11. Johansson, S., Sjösten, P., Nordebo, S. and Claesson, I. Comparison of multiple-and single-reference mimo active noise control approaches using data measured in a dornier 328 aircraft, *International Journal of Acoustics and Vibrations*, **5** (2), 77–88, (2000).